Analysis of electron density distributions from subsystem density functional theory applied to coordination bonds

Samuel Fux, Karin Kiewisch, Christoph R. Jacob *, Johannes Neugebauer *, Markus Reiher

Laboratorium für Physikalische Chemie, ETH Zurich, Wolfgang-Pauli-Strasse 10, 8093 Zurich, Switzerland

ABSTRACT

We investigate the electron density topologies from a subsystem approach to density-functional theory (DFT) for subsystems connected by coordination bonds in comparison to Kohn–Sham–DFT reference calculations. Reasonable results can be obtained for weak dative bonds as in $H_3N \cdots BH_3$ or for bonds with a rather ionic character as in $TiCl_4$. Problems occur for dominant covalent bonding contributions. The subsystem approach shows serious deficiencies in cases of fragments with opposite charge. We show how this problem can be overcome by introduction of a long-distance correction to the embedding potential as recently proposed [C.R. Jacob, S.M. Beyhan, L. Visscher, J. Chem. Phys. 126 (2007) 234116].

© 2008 Elsevier B.V. All rights reserved.

1. Introduction

The electron density can be regarded as a fundamental quantity for the description of matter according to the Hohenberg–Kohn theorem. In addition to quantitative calculations within density functional theory (DFT), recent work also highlights the role of the density for qualitative analyses of electronic structure and an understanding of chemical bonding in molecules, see Refs. [1–3]. These theoretical approaches gain increasing importance in transition metal chemistry; for a review see Ref. [4] as well as the recent studies in Refs. [5,6] and references therein. One interesting aspect of these analyses is the attempt to relate properties of a chemical system to those of certain constituents, e.g., molecules within a supermolecule or functional groups within molecules [7]. That such a decomposition is essential for chemical concepts is apparent in the discussion of coordination compounds in terms of an electron acceptor (e.g., a central metal ion) and electron donating ligands, which becomes manifest in crystal- or ligand-field theory. The electron density can be employed to study the effect of the ligands on the metal center, as has been done in Ref. [8,9] on the basis of subsystem approaches to DFT.

Such subsystem methods aim at obtaining the exact ground-state electron density as a superposition of fragment densities. In the frozen density embedding (FDE) method [10], a partitioning of the density into two fragments is employed: The optimum density ρ_1 of an active subsystem is determined in the presence of an effective embedding potential due to the fixed (frozen) electron density ρ_2 of the environment. By constructing a guess for the environment density ρ_2, one can derive Kohn–Sham-like one-elec-

tron equations for the determination of the optimum density ρ_1 from the minimization of the energy functional $E = E[\rho_1 + \rho_2]$ with respect to ρ_1, while keeping ρ_2 frozen [10,11]. In these one-electron equations for the orbitals $\phi_i^{(1)}$ of system 1, the effect of system 2 is represented by an effective embedding potential $v_{\text{eff}}^{\text{emb}}(\mathbf{r})$, which is given by

$$v_{\text{eff}}^{\text{emb}}[\rho_1, \rho_2](\mathbf{r}) = v_2^{\text{nuc}}(\mathbf{r}) + \int \frac{\rho_2(\mathbf{r}')}{|\mathbf{r}' - \mathbf{r}|}\, d\mathbf{r}' + \frac{\delta E_{\text{xc}}[\rho]}{\delta \rho}\bigg|_{\rho=\rho_{\text{tot}}}$$
$$- \frac{\delta E_{\text{xc}}[\rho]}{\delta \rho}\bigg|_{\rho=\rho_1} + \frac{\delta T_s[\rho]}{\delta \rho}\bigg|_{\rho=\rho_{\text{tot}}} - \frac{\delta T_s[\rho]}{\delta \rho}\bigg|_{\rho=\rho_1}, \quad (1)$$

where $v_2^{\text{nuc}}(\mathbf{r})$ denotes the external potential due to the nuclei of system 2, ρ_{tot} the electron density of the whole system, and E_{xc} and T_s the functionals for the exchange–correlation energy and the kinetic energy for the non-interacting reference system. For the exact functionals $E_{\text{xc}}[\rho]$ and $T_s[\rho]$, this approach would be exact, provided that the exact $\rho_1 = \rho_{\text{tot}} - \rho_2$ is, for a given ρ_2, non-interacting v_s-representable, which also implies that the sought-for ρ_1 is non-negative everywhere in space. Since the v_s-representability condition is in general not fulfilled [11,12], it is usually necessary to optimize both electron densities in an iterative fashion. This can either be done by subsequent embedding calculations with exchanged roles of ρ_1 and ρ_2 [13] or by a simultaneous optimization of all subsystems under study [14,15]. Similar density embedding schemes can also be used in connection with wave function methods [16–20].

The FDE formalism relies on the use of an approximate kinetic-energy functional to describe the non-additive part of the kinetic-energy component of the embedding potential. Approximate kinetic-energy functionals in the FDE scheme have been investigated extensively in the past [21–23], and it was shown that with generalized-gradient approximation (GGA) functionals, accurate results can be obtained for weakly interacting systems

* Corresponding authors.
E-mail addresses: christoph.jacob@phys.chem.ethz.ch (C.R. Jacob), johannes.neugebauer@phys.chem.ethz.ch (J. Neugebauer).

[24–26]. We have recently started a systematic investigation of the electron densities and their topologies from subsystem-DFT in comparison to Kohn–Sham-DFT [12]. To analyze the accuracy of the electron densities obtained from FDE, we have investigated difference and deformation densities, which provide a more sensitive measure than the total electron densities. The difference and deformation densities are defined as $\rho_{super} - \rho_{frag}$ and $\rho_{super} - \rho_{emb}$ where ρ_{super} denotes the electron density obtained from the supermolecular KS-DFT calculation, ρ_{frag} is the superposition of the electron densities of the isolated fragments, and ρ_{emb} is the electron density from the FDE calculation. Furthermore, the distribution of the electron density in the bonding regions has been analyzed by a topological analysis according to the theory of atoms in molecules [1] by locating stationary points of the electron density, in particular the bond critical points (BCPs), which are second-order saddle points of the electron density. The location of the BCPs as well as the value of the electron density $\rho(\mathbf{r})$ and of the negative Laplacian $L(\mathbf{r}) = -\nabla^2\rho(\mathbf{r})$ at this point allows a characterization of the type of the bonding interaction and provides a sensitive measure for the accuracy of the electron density in the bonding region.

We have previously shown that even for very strong hydrogen bonds, such as that in F–H–F$^-$, accurate electron densities can be obtained using subsystem DFT [12]. However for subsystems connected by covalent bonds, the available kinetic-energy functionals are assumed not to be accurate enough, so that a straightforward application of the FDE scheme would not be possible in these cases. Extensions of the FDE scheme have been proposed that can handle such situations, e.g., by the introduction of capping groups, which has been successfully applied to the description of proteins [27].

The aim of this work is to assess the accuracy of the FDE scheme with the currently available approximate kinetic-energy functionals for the case of subsystems connected by coordination bonds. Even though there are a few examples of application of FDE to such systems, e.g., for MnF_6^{4-} [28], lanthanide complexes [8,9], or zinc complexes [29], subsystems connected by donor–acceptor bonds represent a big challenge and push the currently available approximations for the non-additive kinetic energy to their limits. As representative examples of such cases, we will consider ammonia borane, with a dative bond between the nitrogen and the boron atom, and the metal complexes $TiCl_4$ and $Cr(CO)_6$.

2. Computational details

All calculations were performed using the FDE implementation [15,30] in the Amsterdam Density Functional (ADF) package [30–32]. The BP86 exchange–correlation functional [33,34] and the TZP basis set from the ADF basis set library [31] were employed throughout this work. In all FDE calculations, the supermolecular basis set expansion [23], in which the basis functions of both subsystems are employed to expand the subsystem electron densities, was used. The electron densities of both subsystems were relaxed in five freeze-and-thaw [13] cycles. The kinetic-energy component of the embedding potential was approximated using the PW91k generalized-gradient approximation (GGA) kinetic-energy functional, which has the same functional form for the enhancement factor $F(s)$ as the exchange functional of Perdew and Wang [35], and which was parameterized for the kinetic energy by Lembarki and Chermette [36].

In the course of the present work, we discovered an inconsistency in the ADF implementation of the PW91k functional for the spin-restricted case. Instead of using $s = |\nabla\rho|/2\rho k_F$ with $k_F = (3\pi^2\rho)^{1/3}$ as the argument of the enhancement factor $F(s)$, $2^{1/3}s$ was employed yielding an enhancement factor $F(2^{1/3}s)$. This problem also applies to other GGA-type kinetic-energy functionals implemented in ADF, which have, however, hardly been applied.

For details on the definition of the PW91k functional and the corresponding expressions for the spin-restricted and spin-unrestricted case, see Refs. [36,23,37]. This means that the PW91k functional used in previous application of the FDE implementation in ADF effectively corresponds to a 'scaled PW91k' functional with the values $A = 60.575$, $A_1 = 0.074534$, $A_2 = 0.16762$, $A_3 = 0.0510025$ $A_4 = 62.996$, and $B_1 = 0.22925 \times 10^{-4}$ for the parameters in the enhancement factor instead of the original parameters by Lembarki and Chermette [36].

Since the magnitude of the gradient correction to the embedding potential is rather small in most cases, the effect of these scaled parameters in $F(s)$ does not lead to significant changes in molecular properties calculated in earlier work. The changes in the electron densities and negative Laplacians reported in Ref. [12] are ~0.01 $e\,\text{Å}^{-3}$ and <0.1 $e\,\text{Å}^{-5}$, respectively. A re-evaluation of the excitation energies calculated for 220 snapshots of acetone in water [37] showed that the average deviation is smaller than 0.01 eV [19]. The changes in the excitation energies reported for the structure in Fig. 4 in Ref. [30] are of the order of 0.001 eV. Similar results were also observed for examples from the study of pigment molecules in Ref. [38] and the test calculations presented in Ref. [39]. For the water-in-water system investigated in Ref. [40], where both the absolute excitation energies and the solvent shifts are significantly larger, we found somewhat larger deviations of approximately 0.05–0.07 eV; the relative errors in the solvent shifts are about 3–5% and thus still very small. The mean polarizabilities in this system change by less than 0.1 a.u. For the NMR shieldings of the bimolecular complexes studied in Ref. [41] deviations of the order of 0.5 ppm are found. Similar deviations are observed for the solvent shifts reported in Ref. [42], but these errors largely cancel when comparing different solvents.

The electron density and the negative Laplacian $L(\mathbf{r})$ were obtained on a grid of points (step-size 0.01 Å) from a locally modified version of the DENSF-utility program of the ADF package. The search for stationary points in the electron density was performed with the program INTEGRITY [43]. The isocontour plots of the difference densities and $L(\mathbf{r})$ were prepared using a MATHEMATICA script [44,45].

For the supermolecular and the embedding calculations, the contour lines are drawn at 2, 4, $8 \times 10^n\,e\,\text{Å}^{-3}$ for $n = 3, 2, 1, 0, -1, -2$. For the difference density, the contour lines are drawn at ± 2, 4, $8 \times 10^n\,e\,\text{Å}^{-3}$ for $n = -1, -2, -3, -4$. Blue dashed lines indicate negative values, red solid lines indicate positive values and the black line corresponds to a zero difference.

3. FDE electron densities for coordination bonds

3.1. Ammonia borane

The first molecule that was analyzed in this work is ammonia borane. For the FDE calculation the molecule was divided into a BH_3 and a NH_3 fragment. The bond energy between these two subsystems is 187.1 kJ/mol when calculated as the energy difference between the complex and the unrelaxed subsystems with BP86/TZP (no counterpoise correction), which reduces to 133.7 kJ/mol when the subsystems are relaxed, mainly due to structural changes in the BH_3 fragment. The bond energy is thus roughly comparable to F–H–F$^-$, which was the most strongly interacting system discussed in our previous study with a dissociation energy of 185.9 kJ/mol (see Ref. [12] and references therein for details). In F–H–F$^-$, the two subsystems are connected by a very strong hydrogen bond, whereas in ammonia borane the interaction takes place between two uncharged fragments that form a dative bond. The optimized structure of ammonia borane is shown in Fig. 1a. The B–N distance is 1.66 Å (exp.: 1.58 Å [46]).
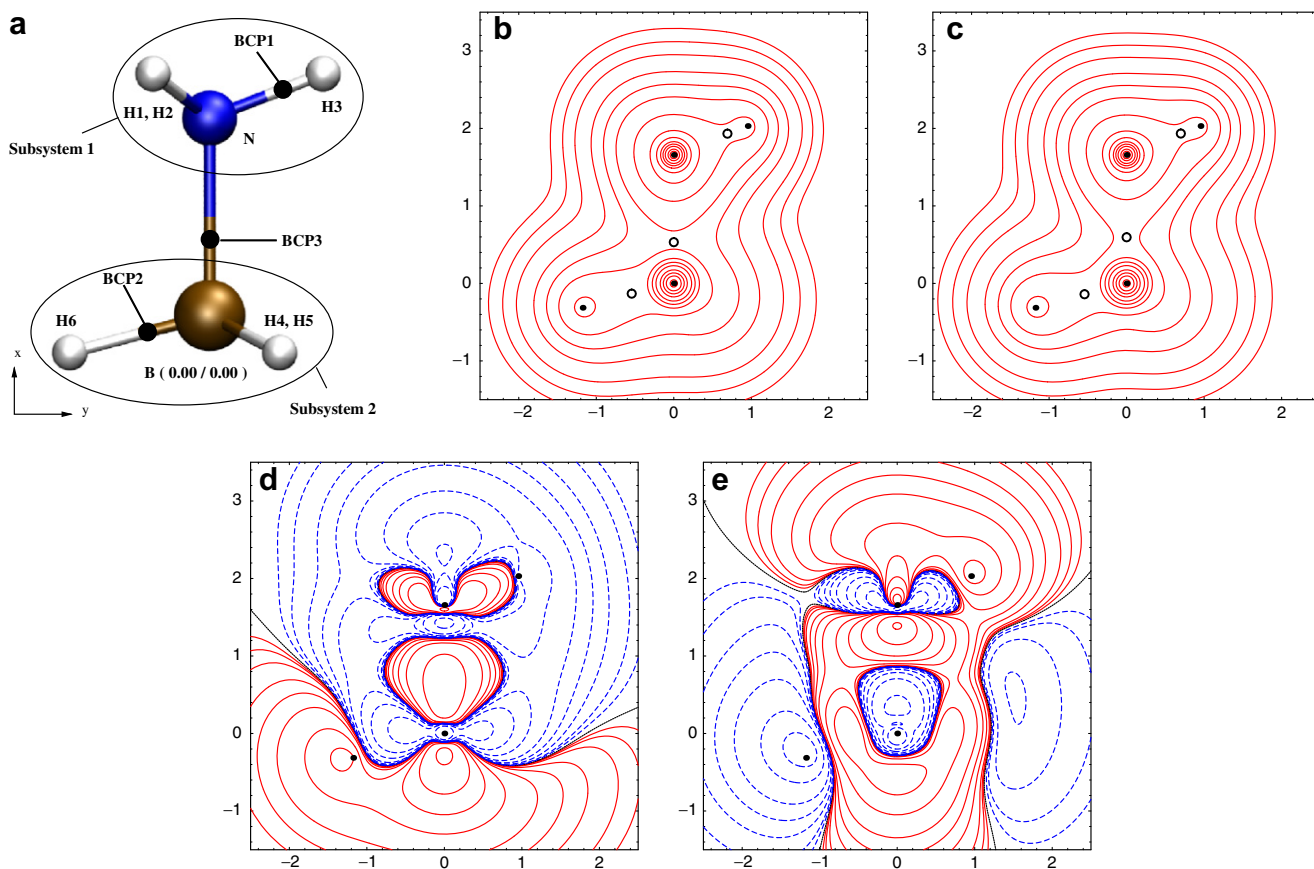
Fig. 1. (a) BP86/TZP optimized structure of ammonia borane (BH_3NH_3). The double labeling of some atoms means that there are two atoms that differ only in their z-coordinate and are therefore overlaying in the picture. Note that the color change along the N–B bond is arbitrary and thus not related to the partitioning into subsystems. (b) Supermolecular density, (c) embedding density, (d) difference density $\rho_{super} - \rho_{frag}$, (e) difference density $\rho_{super} - \rho_{emb}$. The orientation of the molecule in the density plots corresponds to the one of the ball-and-stick model.

Contour plots of the electron density for the supermolecular and the FDE calculation are shown in Fig. 1b and c. The difference of the supermolecular density and the superposition of the isolated fragment densities is shown in Fig. 1d. Significant changes upon bond formation can be observed: The electron density is increased in the bonding region and in the BH_3 moiety, whereas it is decreased around the nitrogen atom. An exception is a ring of increased electron density around the nitrogen atom that is perpendicular to the bonding axis. The difference of the supermolecular density and the density from the FDE calculation is shown in Fig. 1e. The differences on the bonding axis are smaller than in Fig. 1d, which means that FDE works qualitatively correct and shifts electron density towards the bonding axis, although there are still some deficiencies. This can also be seen from the dipole moments obtained in these calculations, which are 5.34 D for the supermolecular case, 2.08 D for the sum of the dipole moments of the isolated fragments, and 6.75 D for FDE. The embedding scheme thus qualitatively reproduces changes in the dipole moment upon bond formation, but overestimates the value from the supermolecular calculation.

The values for the electron density and the negative Laplacian at the BCPs are shown in Table 1. The difference of the supermolecular density and the superposition of the isolated fragment densities at BCP3, which is located at the border of the two subsystems, is 0.2753 e Å^{-3}, which means that there are large changes upon the formation of the bond. By comparing the coordinates of BCP3, one notices that the x-coordinate of BCP3 is shifted towards the nitrogen atom by the FDE scheme, whereas the other BCPs are al-

Table 1
Coordinates $\boldsymbol{r}_{BCP}$ (in units of Å) of the BCPs and values of $\rho(\mathbf{r})$ in e Å^{-3} and $L(\mathbf{r})$ in e Å^{-5} at the bond critical points of ammonia borane

		$\boldsymbol{r}_{x,BCP}$	$\boldsymbol{r}_{y,BCP}$	$\rho(r)$	$L(r)$
BCP 1	Super	1.93	0.69	2.22	9.59
	Emb	1.93	0.70	2.22	10.00
	Diff	0.00	−0.01	0.00	−0.41
BCP 2	Super	−0.13	−0.54	1.12	2.27
	Emb	−0.14	−0.54	1.06	1.67
	Diff	−0.01	0.00	0.06	0.60
BCP 3	Super	0.53	0.00	0.71	−1.77
	Emb	0.60	0.00	0.87	1.09
	Diff	−0.07	0.00	−0.16	−2.86

most unchanged. The shift of 0.07 Å for BCP3 is larger than the shifts that were observed in Ref. [12] in the analysis of hydrogen-bonded systems with FDE. Regarding the difference density, one can observe that the value of the electron density from the FDE calculation is too low in the region around H3, whereas in the region around H6, it is too high.

The difference density at BCP3 is an order of magnitude larger than the difference density at BCP1 and BCP2, which are located in the center of their corresponding fragments. Compared to the superposition of the isolated fragment densities at BCP3 (0.4382 e Å^{-3}) we note that FDE works qualitatively correctly but overcorrects the density in this region. Also the error in the negative Laplacian at BCP3 differs considerably from the values of BCP1

and BCP2. Compared to the analysis of hydrogen bonded systems in Ref. [12], the difference of the electron density in the boundary region of the two subsystems is not very large, but the discrepancies in the negative Laplacian are more pronounced. The sign of the negative Laplacian is an indicator for the type of bonding in a molecule [1]. One would expect a positive sign for a covalent bond, but not for a coordination bond. The negative Laplacian at BCP3 is positive for FDE but negative for the supermolecular calculation, which means that the bonding region is not described entirely correctly. In summary, ammonia borane represents a more challenging system for FDE than the previously studied hydrogen bonded systems although qualitative changes in the electron density upon bond formation are described correctly.

3.2. TiCl$_4$

Titaniumtetrachloride is a tetrahedral complex with T_d symmetry and even stronger interactions between the central metal atom and the ligands. The optimized structure is shown in Fig. 2a. The Ti–Cl distance is 2.19 Å (exp.: 2.18 Å) and the Cl–Ti–Cl angle is 109.47°. The reference data were taken from Ref. [47]. For the FDE calculation, the complex was divided into a negatively charged Cl$^-$ and a positively charged TiCl$_3^+$ fragment. Initial FDE calculations converged very slowly and the electron density obtained was unreasonable. If TiCl$_3^+$ was treated as the frozen fragment, a spurious charge transfer from the Cl$^-$ fragment to the TiCl$_3^+$ fragment took place. The SCF procedure for the TiCl$_3^+$ fragment only converged if one enforced a non-aufbau solution with one unoccupied

orbital with a lower orbital energy than the highest occupied molecular orbital (HOMO). These difficulties are due to a well-known problem of the FDE embedding potential at the frozen system [48], in particular close to the nucleus. The problem originates from the inability of the available GGA kinetic-energy functionals to compensate the large nuclear attraction sufficiently. In earlier examples this incorrect behavior caused a wrong orbital ordering only at a very large distance between the subsystems. The present example demonstrates that for certain choices of subsystems the embedding potential fails to produce the correct orbital occupation even at the equilibrium distance. A practical solution to this problem was suggested in Ref. [48] by applying a position-dependent correction that enforces the correct behavior of the embedding potential at the frozen subsystem. This long-distance correction resulted in an aufbau solution with the expected order of orbitals in our case, i.e., the spuriously low-lying orbital was shifted to higher energies.

Contour plots of the electron density for the supermolecular and the FDE calculation are shown in Fig. 2b and c. The difference of the supermolecular density and the superposition of the densities of the isolated fragments is shown in Fig. 2d. Due to the complex formation, electron density is transferred from the Cl$^-$ fragment towards the titanium atom. The most important change occurs in the center of the TiCl$_3^+$ fragment. The difference of the supermolecular density and the density from the FDE calculation is shown in Fig. 2e. Near the titanium atom the electron density from the FDE calculation is too low, whereas it is too high at Cl1 perpendicular to the Ti–Cl bond. Also in the center of the Ti–Cl2
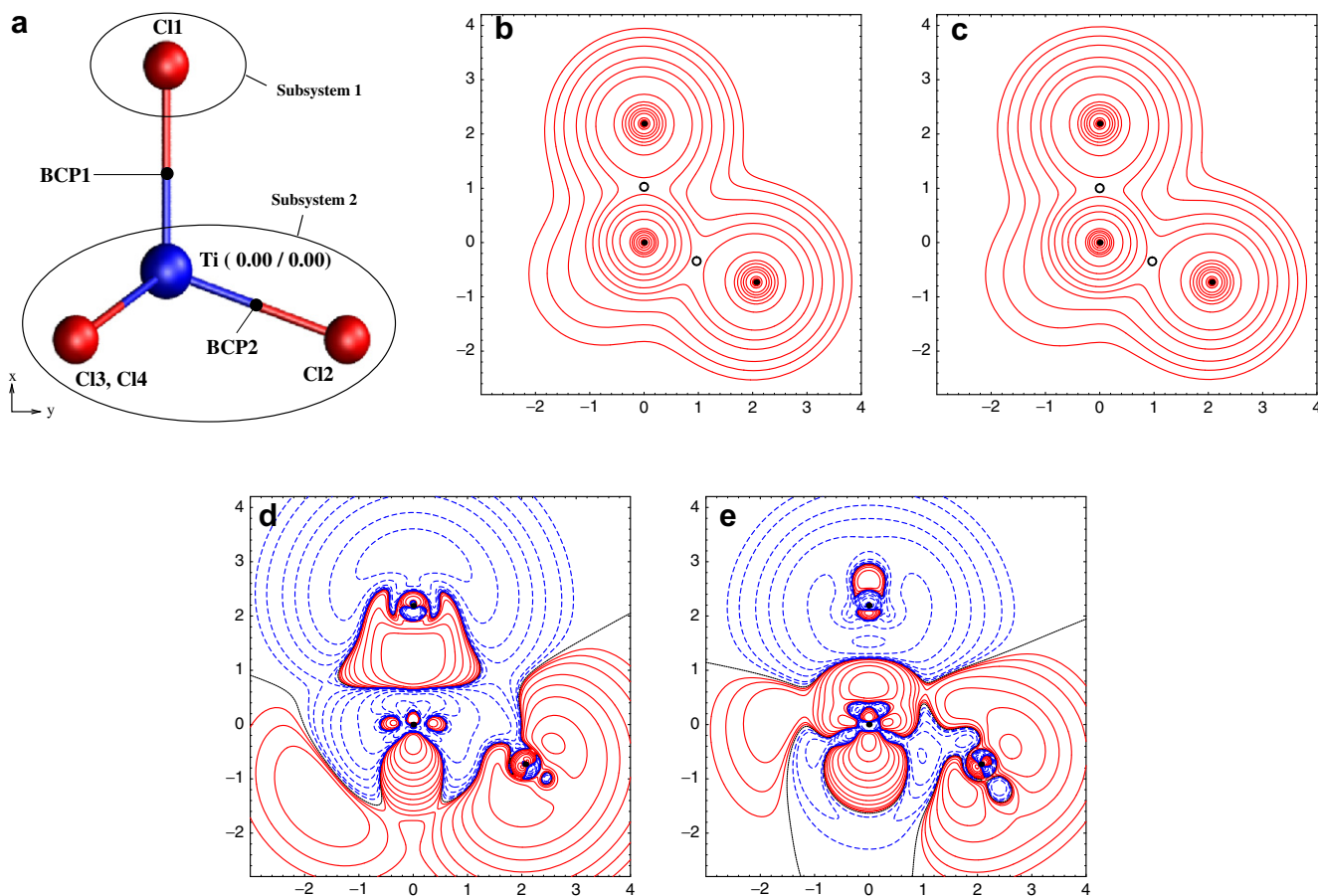
Fig. 2. (a) BP86/TZP optimized structure of titaniumtetrachloride. The double labeling of some atoms means that there are two atoms, that differ only in their *z*-coordinate and are therefore overlaying in the picture. Note that the color change along the Ti–Cl bond is arbitrary and thus not related to the partitioning into subsystems. (b) Supermolecular density, (c) embedding density, (d) difference density $\rho_{super} - \rho_{frag}$, (e) difference density $\rho_{super} - \rho_{emb}$. The orientation of the molecule in the density plots corresponds to the one of the ball-and-stick model.

Table 2
Coordinates $\mathbf{r}_{BCP}$ (in units of Å) of the BCPs and values of $\rho(\mathbf{r})$ in $e\,\text{Å}^{-3}$ and $L(\mathbf{r})$ in $e\,\text{Å}^{-5}$ at the bond critical points of titaniumtetrachloride

		$\mathbf{r}_{x,BCP}$	$\mathbf{r}_{y,BCP}$	$\rho(r)$	$L(r)$
BCP 1	Super	1.03	0.00	0.65	−1.73
	Emb	1.00	0.00	0.59	−2.34
	Diff	0.03	0.00	0.06	0.61
BCP 2	Super	−0.34	0.97	0.65	−1.73
	Emb	−0.35	0.97	0.66	−1.68
	Diff	0.01	0.00	−0.01	−0.05

bonding region FDE overestimates the electron density, although the differences are small.

The values for the electron density and the negative Laplacian are shown in Table 2. At BCP1 near the border of the two subsystems the difference of the supermolecular density and the electron density from the FDE calculation and the difference of the negative Laplacian are rather small ($\sim$0.06 $e\,\text{Å}^{-3}$ and 0.61 $e\,\text{Å}^{-5}$, respectively); at BCP2 these deviations are even smaller. The negative Laplacian has the correct sign at both BCPs. The values of the difference density in titaniumtetrachloride are significantly smaller than in ammonia borane. Moreover, there is only a slight shift in the x-coordinate of BCP1.

3.3. Cr(CO)$_6$

The octahedral complex chromium hexacarbonyl is a prototypical example of a metal complex in which π-backdonation plays an important role, and which thus cannot be entirely understood in terms of simple ligand field theory. The optimized structure is shown in Fig. 3a. The Cr–C distance is 1.91 Å (exp.: 1.91 Å) and the C–O distance is 1.16 Å (exp.: 1.14 Å). The reference data were taken from Ref. [49]. The electronic structure expected for chromium in a strong octahedral ligand field would be [Ar]$(t_{2g})^6$. The FDE calculation converged to an aufbau solution with the unexpected configuration [Ar]$(a_{1g})^2(e_g)^4$, caused by additional low-lying orbitals centered on the ligands. Note that the non-additive kinetic energy part of the potential should actually destabilize such ligand orbitals in the calculation of the Cr fragment in order to mimic the Pauli repulsion with the occupied orbitals in the (CO)$_6$ fragment. Apparently, this destabilizing effect is too weak in the present example. This is again related to the deficiency of the available GGA kinetic-energy functionals discussed above. The electron density for this electronic structure is unreasonable, because it is very similar to the density of the superposition of the isolated fragments, except in the region around the chromium atom. The same calculation was performed enforcing the correct occupation, which resulted in a non-aufbau solution for chromium with the electronic configuration [Ar]$(a_{1g})^0(t_{1u})^0(t_{2g})^6$.

By applying the long-distance correction suggested in Ref. [48], the number of unoccupied orbitals that are lower in energy than the HOMO could be reduced. It was, however, not possible to obtain an aufbau solution with the expected occupation scheme. A set of three t_{1u} orbitals and one a_{1g} orbital were still found to be lower in energy than the metal-centered t_{2g} orbital. These orbitals are shown in Fig. 4a and b for the calculation without
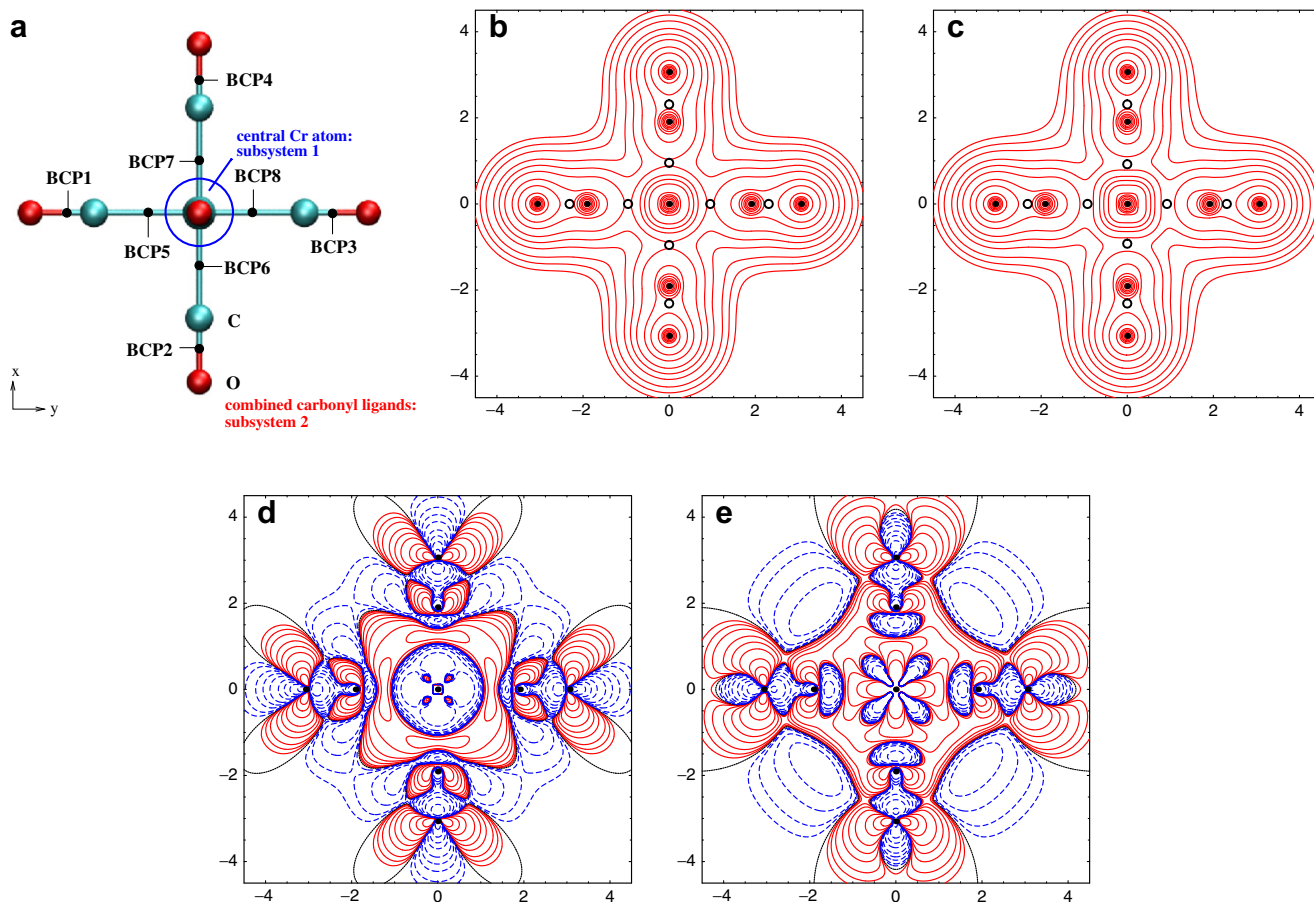
Fig. 3. (a) BP86/TZP optimized structure of chromium hexacarbonyl. Note that the color change along the Cr–C bond is arbitrary and thus not related to the partitioning into subsystems. (b) Supermolecular density, (c) embedding density, (d) difference density $\rho_{super} - \rho_{frag}$, (e) difference density $\rho_{super} - \rho_{emb}$. The orientation of the molecule in the density plots corresponds to the one of the ball-and-stick model.
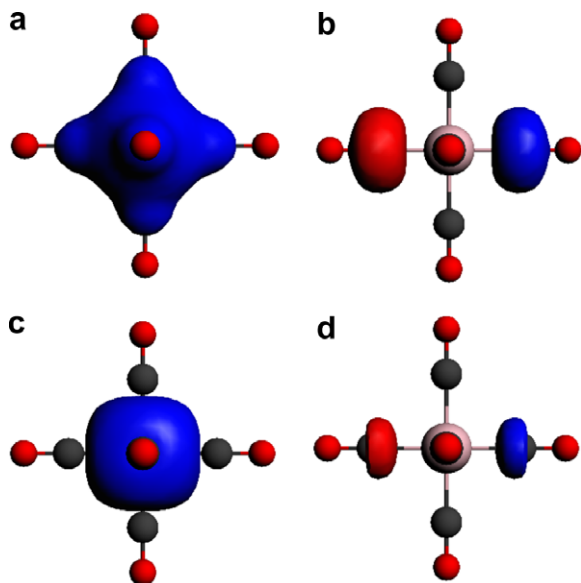
Fig. 4. (a) Low-lying a_{1g} orbital from the FDE calculation on $Cr(CO)_6$ without long-distance correction (contour value = 0.045), (b) one of the three low-lying t_{1u} orbitals from the calculation without the long-distance correction (contour value = 0.05), (c) the orbital corresponding to the one shown in (a) from the calculation with the long-distance correction (contour value = 0.045), (d) the orbital corresponding to the one shown in (b) from the calculation with the long-distance correction (contour value = 0.05).

the long-distance correction, and in Fig. 4c and d for the calculation with the correction. The orbitals are located on the carbon atoms of the carbonyl ligands. The long-distance correction leads to a contraction of these orbitals by raising the potential in the region of the ligand atoms. The rather sharp boundary in the isosurface plot can be explained in terms of the distance-dependence of the long-distance correction.

It should be noted that the destabilizing effect of this correction could be modified by changing the parameter α in Eq. (34) of Ref. [48], which controls the threshold to switch on the correction terms. However, it seems unreasonable to further tune this parameter since the correction enforces a limit that is only correct at large separations of the subsystems.

The supermolecular and the embedding densities are shown in Fig. 3b and c. The difference density is shown in Fig. 3d. In contrast to most other examples studied in this work and in Ref. [12], already the electron densities show significant differences and no sophisticated topological analysis is needed in this case to reveal the deficiencies of the subsystem approach.

4. Conclusions

In this work we have investigated the electron density distributions from FDE calculations on subsystems connected by coordination bonds. We have considered cases that pose serious challenges on the embedding approach due to the fact that covalent contributions to the bonds become important. It was found that the electron density in the B–N bonding region in ammonia borane can be reasonably well described, although its Laplacian points to a wrong type of bonding. For the bonding in $TiCl_4$, we experienced difficulties with the embedding approach for charged fragments when used in a naive way, which are due to the known deficiencies of the embedding potential at the frozen subsystem. We have shown that these problems, that result in an unphysical charge transfer from Cl^- to $TiCl_3^+$, can be overcome in a pragmatic way by applying the long-distance correction suggested in Ref. [48]. In that way, a good agreement of the electron density and its neg-

ative Laplacian from FDE at the BCPs with the corresponding reference values from a Kohn–Sham DFT calculation could be achieved.

The same approach was helpful in the attempt to employ FDE for systems with stronger interactions for which orbital overlap effects play an important role, e.g., the π-backdonation in carbonyl complexes like chromium hexacarbonyl. Also here, the initial results obtained with current approximations to the kinetic-energy component of the embedding potential were not reliable, since the expected orbital order could not be reproduced. Ligand-centered orbitals appeared at too low energies in the calculation on the metal subsystem, and the density distribution consequently showed qualitative errors. This could partly be remedied with the long-distance correction from Ref. [48], although two sets of low-lying ligand-centered orbitals still remained. If the correct occupation of the orbitals for the Cr fragment is enforced, the result is a non-aufbau solution that still shows large discrepancies in comparison to the supermolecular Kohn–Sham calculation. A possible explanation for this remaining deviation is the rather large covalent contribution to the Cr–C bond due to the π-backdonation of the carbonyl ligands.

For the applicability of the FDE method we can thus recognize a clear trend. In Ref. [12] it has been shown that for van der Waals complexes, the FDE approach is very successful and it also works well for weak hydrogen bonds. Even for strongly hydrogen-bonded systems like F–H–F$^-$ a good description can be achieved. In this work we showed that coordination bonds represent borderline cases. Whereas weak dative bonds or bonds with strongly ionic character are described reasonably well, FDE fails for coordination compounds with strong covalent bonding contributions with currently available approximations for the kinetic-energy component of the embedding potential.

The conclusions of this work point to some important directions for the development of improved approximations to the kinetic energy component of the embedding potential. The examples show that the accurate description of the embedding potential at the frozen subsystem, in particular near the nuclei, is important to obtain a description that is at least qualitatively correct, i.e., that gives the correct orbital order. It was shown that the simple correction proposed in Ref. [48] works into the right direction for the system considered here. However, it should be noted that this correction contains terms that are explicitly position-dependent, while approximations in terms of the density only would be preferable. The systems studied here will be crucial for the validation of future developments, like the most recent improved density functional approximation to the kinetic energy component of the embedding potential [50], which enforces the exact behavior near the nuclei of the frozen subsystem.

Acknowledgments

References

[1] R. Bader, Atoms in Molecules, Clarendon Press, Oxford, 1990.
[2] P. Geerlings, F. De Proft, W. Langenaeker, Chem. Rev. 103 (2003) 1793.
[3] R.F. Nalewaski, P.W. Ayers, R.G. Parr, From Molecular Structure to Chemical Reactivity: The Density-Functional Perspective, Oxford University Press, Oxford, in press.
[4] W. Scherer, G.S. McGrady, Angew. Chem., Int. Ed. 43 (2004) 1782.
[5] G. Eickerling, R. Mastalerz, V. Herz, H.-J. Himmel, W. Scherer, M. Reiher, J. Chem. Theory Comput. 3 (2007) 2182.
[6] G. Eickerling, M. Reiher, J. Chem. Theory Comput. 4 (2008) 286.

 [7] M. Reiher, Found. Chem. 5 (2003) 23.
 [8] M. Zbiri, M. Atanasov, C. Daul, J.M. García-Lastra, T.A. Wesolowski, Chem. Phys. Lett. 397 (2004) 441.
 [9] M. Zbiri, C. Daul, T.A. Wesolowski, J. Chem. Theory Comput. 2 (2006) 1106.
[10] T.A. Wesolowski, A. Warshel, J. Phys. Chem. 97 (1993) 8050.
[11] T.A. Wesolowski, One-electron equations for embedded electron density: challenge for theory and practical payoffs in multilevel modelling of complex polyatomic systems, in: J. Leszczynski (Ed.), Computational Chemistry: Reviews of Current Trends, vol. 10, World Scientific, Singapore, 2006.
[12] K. Kiewisch, G. Eickerling, M. Reiher, J. Neugebauer, J. Chem. Phys. 128 (2008) 044114.
[13] T.A. Wesolowski, J. Weber, Chem. Phys. Lett. 248 (1996) 71.
[14] M. Iannuzzi, B. Kirchner, J. Hutter, Chem. Phys. Lett. 421 (2006) 16.
[15] C.R. Jacob, J. Neugebauer, L. Visscher, J. Comput. Chem. 29 (2008) 1011.
[16] N. Govind, Y.A. Wang, A.J.R. da Silva, E.A. Carter, Chem. Phys. Lett. 295 (1998) 129.
[17] T. Klüner, N. Govind, Y.A. Wang, E.A. Carter, Phys. Rev. Lett. 86 (2001) 5954.
[18] P. Huang, E.A. Carter, J. Chem. Phys. 125 (2006) 084102.
[19] A.S.P. Gomes, C.R. Jacob, L. Visscher, Phys. Chem. Chem. Phys., in press, doi:10.1039/b805739g.
[20] T.A. Wesolowski, Phys. Rev. A 77 (2008) 012504.
[21] T.A. Wesolowski, H. Chermette, J. Weber, J. Chem. Phys. 105 (1996) 9182.
[22] T.A. Wesolowski, J. Weber, Int. J. Quant. Chem. 61 (1997) 303.
[23] T.A. Wesolowski, J. Chem. Phys. 106 (1997) 8516.
[24] C.R. Jacob, T.A. Wesolowski, L. Visscher, J. Chem. Phys. 123 (2005) 174104.
[25] T.A. Wesolowski, Y. Ellinger, J. Weber, J. Chem. Phys. 108 (1998) 6078.
[26] F. Tran, J. Weber, T.A. Wesolowski, Helv. Chim. Acta 84 (2001) 1489.
[27] C.R. Jacob, L. Visscher, J. Chem. Phys. 128 (2008) 155102.
[28] J.M. García-Lastra, T. Wesolowski, M.T. Barriuso, J.A. Aramburu, M. Moreno, J. Phys.: Condens. Mat. 18 (2006) 1519.
[29] G. Hong, M. Strajbl, T.A. Wesolowski, A. Warshel, J. Comput. Chem. 21 (2000) 1554.
[30] J. Neugebauer, C.R. Jacob, T.A. Wesolowski, E.J. Baerends, J. Phys. Chem. A 109 (2005) 7805.
[31] Amsterdam Density Functional Program, Theoretical Chemistry, Vrije Universiteit, Amsterdam, URL: <http://www.scm.com>.
[32] G. te Velde, F.M. Bickelhaupt, E.J. Baerends, C. Fonseca Guerra, S.J.A. van Gisbergen, J.G. Snijders, T. Ziegler, J. Comput. Chem. 22 (2001) 931.
[33] A.D. Becke, J. Chem. Phys. 98 (1993) 5648.
[34] J.P. Perdew, Phys. Rev. B 33 (1986) 8822.
[35] J.P. Perdew, in: P. Ziesche, H. Eschrig (Eds.), Electronic Structure of Solids, Akademie Verlag, Berlin, 1991.
[36] A. Lembarki, H. Chermette, Phys. Rev. A 50 (1994) 5328.
[37] J. Neugebauer, M.J. Louwerse, E.J. Baerends, T.A. Wesolowski, J. Chem. Phys. 122 (2005) 094115.
[38] J. Neugebauer, J. Phys. Chem. B 112 (2008) 2207.
[39] J. Neugebauer, J. Chem. Phys. 126 (2007) 134116.
[40] C.R. Jacob, J. Neugebauer, L. Jensen, L. Visscher, Phys. Chem. Chem. Phys. 8 (2006) 2349.
[41] C.R. Jacob, L. Visscher, J. Chem. Phys. 125 (2006) 194104.
[42] R.E. Bulo, C.R. Jacob, L. Visscher, J. Phys. Chem. A 112 (2008) 2640.
[43] C. Katan, P. Rabiller, C. Lecomte, M. Guezo, V. Oison, M. Souhassou, J. Appl. Crystallogr. 36 (2003) 65.
[44] Wolfram Research, Inc., Mathematica Version 5.2, Wolfram Research, Inc.: Champaign, Illinois, 2005.
[45] M. Presnitz, F. Mayer, V. Herz, G. Eickerling, W. Scherer, calc.lap.nb: A Mathematica Script for the Analysis of Charge Density Distributions, Universität Augsburg (Lehrstuhl CPM), 2007.
[46] W.T. Klooster, T.F. Koetzle, P.E.M. Siegbahn, T.B. Richardson, R.H. Crabtree, J. Am. Chem. Soc. 121 (1999) 6337.
[47] M.W. Lister, L.E. Sutton, Trans. Faraday Soc. 37 (1941) 393.
[48] C.R. Jacob, S.M. Beyhan, L. Visscher, J. Chem. Phys. 126 (2007) 234116.
[49] L.J. Farrugia, C. Evans, J. Phys. Chem. A 109 (2005) 8834.
[50] J.M. García-Lastra, J.W. Kaminski, T.A. Wesolowski, Preprint available at arXiv:physics.chem-ph/0804.0602, 2008.